Influence of Cardiac Fiber Orientation on Wavefront Voltage, Conduction Velocity, and Tissue Resistivity in the Dog

DAVID E. ROBERTS, LAWRENCE T. HERSH, AND ALLEN M. SCHER

SUMMARY When the canine epicardium is stimulated, the spread of epicardial excitation is 2.4 times faster parallel to the long axes of the cardiac fibers than perpendicular to them. Likewise, gross tissue resistivity is lower parallel to fibers by a factor of 3.2, and the voltage across the depolarization wave is approximately three times as great in the longitudinal direction. Equations are presented which relate these variables. Theoretical considerations confirm the experimental finding that the potentials around a wave of depolarization cannot be accounted for by the conventional hypothesis that the wavefront is a uniform double-layer current source. *Circ Res 44: 701-712, 1979*

AN UNDERSTANDING of electrocardiographic potentials during ventricular depolarization would be demonstrated if it were possible to predict body surface potentials during the QRS complex from a knowledge of the successive positions of boundaries between resting and depolarized myocardium (isochrones). Relating body surface potentials to isochrone position requires, among other things, a knowledge of the electrical generator strength across the isochrone and a knowledge of myocardial electrical resistivity. Isochrone position is determined by the anatomy of the ventricles, including that of the specialized conducting tissue, by the velocity of depolarization in these myocardial tissues, and by the site(s) of initial depolarization. From data in the literature, it appears that there are effects of cardiac fiber direction on conduction velocity, on resistivity, on generator (wavefront) strength, and on the potentials generated by a wave of depolarization. This paper is concerned with these effects.

Myocardial conduction velocity has been measured in several preparations, but there are some differences and variability in the reported velocities (Sano et al., 1959; Draper and Mya-Tu, 1959; Weidmann, 1970; Clerc, 1976). In some experiments, wavefront velocity has been reported to be influenced by fiber direction (Sano et al., 1959; Draper and Mya-Tu, 1959; Clerc, 1976), but in several studies of depolarization in the intact ventricle, fiber direction has not been considered (Scher and Young, 1957; Durrer et al., 1970; Sodi-Pallares, 1956).

From the Department of Physiology and Biophysics, University of Washington School of Medicine, Seattle, Washington.

Supported by Research Grant HL 20273-02 from the National Heart, Lung, and Blood Institute, National Institutes of Health.

Address for reprints: Dr. Allen M. Scher, Department of Physiology and Biophysics (SJ-40), University of Washington School of Medicine, Seattle, Washington 98195.

Received August 22, 1978; accepted for publication November 21, 1978.

Weidmann (1970) and Plonsey (1974) have noted that the extracellular potential drop across a depolarization wavefront (wavefront voltage) is determined by the magnitude of the membrane action potential and by the ratio of extracellular to intracellular resistivity. This connection between potential drop and resistivity has been used to determine resistivity (Weidmann, 1970) and to determine the relationship between muscle fiber orientation, extracellular and intracellular resistivities, and longitudinal (parallel to muscle fibers) and transverse (perpendicular to fibers) velocities (Clerc, 1976). The values of wavefront voltage in these in vitro studies appear low compared with those observed in the heart in situ (Corbin and Scher, 1977; Vander Ark and Reynolds, 1970; Spach and Barr, 1976; Selvester et al., 1970). The values of resistivity reported from in vitro preparations (Weidmann, 1970; Clerc, 1976) also differ substantially from values reported for the heart in situ (Rush et al., 1963).

The effects of the variation of wavefront voltage with fiber direction as a factor in the understanding of the origin of extracellular potentials have not been extensively studied. However, a previous study from our laboratory (Corbin and Scher, 1977) indicated that fiber direction is important in determining potentials at a distance from the electrical sources. In that study, an empirical model was proposed for the dependence of wavefront strength on fiber orientation. That model, referred to as the "axial hypothesis," differed markedly from the uniform double-layer theory (Frank, 1953), which postulated a uniform wavefront strength. The axial hypothesis was a useful first step in understanding the effect of fiber direction on wavefront strength, but it probably predicted too strong a dependence of wavefront voltage on fiber orientation. Clerc (1976) has provided a basis for understanding this dependence, but he did not address the consequences for the understanding of electrocardiographic potentials. Several previous studies (Sano

Downloaded from http://ahajournals.org by on March 12, 2022

et al., 1959; Draper and Mya-Tu, 1959; Clerc, 1976) have given information only about purely longitudinal or purely transverse excitation waves, whereas the excitation waves in a normally beating heart generally are not purely longitudinal or transverse.

Experiments reported here deal with the spread of excitation and resultant potential fields following left ventricular epicardial stimulation applied to the central terminal of an epicardial electrode array covering an area of 9 × 16.5 mm. We have used this array to (1) map successive positions of the wavefront to determine the velocity of epicardial conduction with respect to fiber direction, (2) map potentials on the epicardial surface for several positions of the isochrone and note the effect of cardiac fiber direction on these maps, (3) map voltage across the wavefront and its relationship to fiber direction, and (4) map the potential induced at recording points of the array by current injection at a central terminal to determine electrical resistivity. From the above we can draw some conclusions about the wavefront voltage in myocardium. We also present a theoretical framework that allows us to relate conduction velocity, tissue resistivity, and wavefront voltage.

Methods

Experiments were conducted in nine mongrel dogs weighing 20–34 kg. The dogs were anesthetized with morphine (1 mg/kg, im) followed by chloralose (75–100 mg/kg iv, supplemented as needed) and were positioned on their right sides. A thoracotomy was performed between the 4th and 5th ribs, the pericardium was opened, and the heart was exposed.

Potentials were recorded from a multiterminal epicardial electrode consisting of 84 terminals of silver wire 0.25 mm in diameter embedded in plastic in a rectangular flat array with a spacing of 1.5 mm in each direction. A switch connected either seven or 14 of the terminals to the recording system simultaneously. The electrode was held against the ventricular epicardium by hand. The heart was kept moist with normal saline, but the area beneath and surrounding the electrode was wiped with a saline-soaked pad before the electrode was applied. Our purpose was to remove fluid that would have furnished an extraneous current path. Probably most of this fluid was removed, because the electrode was held against the heart (this is discussed below). Stimulation was applied at the central terminal (Fig. 1). The stimulus was just above threshold, 0.25–3 msec in duration, at a rate just exceeding the natural heart rate. Potentials were recorded with respect to an indifferent electrode at a remote site in the thoracic opening. During normally conducted beats, the injury potential averaged over all recording terminals was less than 1 mV, indicating the absence of injury sufficient to distort the measured waveforms.

Sharpened stainless steel pins 0.3 mm in diameter were sometimes inserted into the myocardium through holes in the corners of the epicardial electrode to prevent movement. In three of the hearts, the tissue was fixed with pins in place. This made it possible to determine fiber orientation and to relate it to electrode position when the tissue was sectioned later. For the other electrode positions, epicardial fiber direction was assumed to correspond to the direction of maximal epicardial conduction velocity, as it did in the hearts from which histological sections were made. Serial sections of the tissue at 1-mm intevals showed rotation of the fiber direction with depth, consistent with reports in the literature (Armour and Randall, 1970; Streeter et al., 1969). The epicardial fiber direction seen on inspection of the heart in situ generally agreed well with the direction shown by sections and with the direction of maximal conduction velocity, but results of visual inspections were not used in analysis.

The amplified potentials were recorded on magnetic tape by a digital computer. Analog-to-digital conversion was at 12-bit accuracy at 1000 samples/sec (four dogs) or 2000 samples/sec (five dogs). Time alignment of the digitized waveforms was achieved by a trigger synchronous with the stimulus recorded along with the waveforms on the digital tape. The voltage immediately before stimulation was used as the baseline. For each electrode position, a computer program printed time of activity, voltage drop across the wave, and potential maps at 1-msec intervals.

Reproducibility was tested by making repeated maps of time of activity, potential across the wavefront, and potential distribution for the same electrode position for different heart beats. Times of activity generally were reproducible to within 1 msec for 1000/sec sampling or 0.5 msec for 2000/sec sampling. This error is due to the lack of synchronization between the stimulus and the computer sampling pulses. In two experiments, we synchronized the stimulus with the computer sampling pulses. With this synchronization and with short (0.25-msec) stimuli, we found that beat-to-beat variation in the time of activity was eliminated at the time resolution (0.5 msec) available with a sampling rate of 2000/sec. Local depolarization was considered to occur when the maximal rate of change of potential occurred at each recording terminal. Isochrones were drawn connecting points simultaneously depolarized (Fig. 1).

The wavefront voltage was taken to be the maximal difference between two voltage samples 2 msec apart. The considerations that led to this choice are presented in the Discussion.

We determined gross tissue resistivity by constructing maps of the stimulus artifact potential produced by a rectangular pulse-current source. For these measurements, we used an isolated stimulator

Downloaded from http://ahajournals.org by on March 12, 2022

with an output impedance in excess of 100 MΩ. This prevented any influence of stimulating electrode polarization on the magnitude of the stimulation current. The current was monitored by recording the voltage across a precision (± 1%) 1000-Ω resistor in series with the stimulator output. We checked the method by measuring the resistivity of a solution of known concentration of potassium chloride. For 10 and 40 mM KCl at 25°C, the resistivities averaged over the 83 recording points of the epicardial array were 689 ± 30 and 182 ± 13 Ω-cm, respectively, compared with the expected (MacInnes, 1961) values of 708 and 187 Ω-cm. In Appendix F, the formula used for calculating resistivity from maps of stimulus artifact magnitude (such as in Fig. 5) is presented. Sensitivity to the placement of indifferent recording and current injection electrodes was tested by moving these electrodes about widely on the dog's body. Changes in indifferent electrode placement resulted in changes of measured resistivity of up to 5%. This systematic error is of about the same magnitude as the variation in resistivity from heart to heart (see Results). Resistivity was measured in five of the nine dogs studied.

For the sake of simplicity, Figures 1 through 5 are all from one electrode position on the basal left ventricle of one dog.

All error limits are given here in terms of the standard deviation. The acquisition, editing, and processing of data described above were performed on a laboratory minicomputer, the LM[2] (Kehl et al., 1975).

Theoretical Considerations

We present equations which elaborate a recent theoretical analysis by Clerc (1976) as a basis for unifying measurements of conduction velocity, resistivity, and wavefront voltage. Clerc's analysis relates the anisotropy of conduction velocity and wavefront voltage to the intracellular and extracellular resistivities for cross-fiber (transverse) and parallel-to-fiber (longitudinal) current flow. The formulas given here are extensions of those of Clerc and are verified in Appendix C. The first equation indicates that the extracellular potential drop $V_o(\gamma)$ across a plane depolarization wavefront is a function of the angle γ between the local fiber direction and the perpendicular to the wavefront, and of tissue resistivities:

$$V_o(\gamma) = \frac{V_{ol}\cos^2\gamma + (r_l/r_t)V_{ot}\sin^2\gamma}{\cos^2\gamma + (r_l/r_t)\sin^2\gamma}. \quad (1)$$

Here, r_l and r_t are the longitudinal and transverse tissue resistivities, V_{ol} is the extracellular potential drop across a longitudinal ($\gamma = 0°$) wave, and V_{ot} is the potential drop across a transverse ($\gamma = 90°$) wave.

The uniform double-layer theory (Frank, 1953) predicts a constant potential drop for a wave moving in any direction; i.e., V_{ot} would equal V_{ol} in Equation 1. Equation 2 shows, however, that the anisotropy of conduction velocity (Draper and Mya-Tu, 1959) and tissue resistivity (Rush et al., 1963) in mammalian ventricle necessarily imply an anisotropic wavefront voltage:

$$V_{ot} = \frac{1}{2}\Delta\left\{1 - \left[1 - 4\frac{V_{ol}}{\Delta}\left(1 - \frac{V_{ol}}{\Delta}\right)\left(\frac{v_t}{v_l}\right)^2\frac{r_t}{r_l}\right]^{\frac{1}{2}}\right\}. \quad (2)$$

V_{ol}, V_{ot}, r_l, and r_t have been defined in the paragraph above; Δ is the membrane action potential ($\simeq$100 mV); and v_t and v_l are the transverse and longitudinal conduction velocities, respectively. The potential drops $V_o(\gamma)$ and V_{ot} are expressed here in this form because each of the variables on the right side of Equation 1 and 2 were directly measured in this study. These two formulas enable us to determine wavefront voltage for any angle of wavefront propagation from measurements of velocity, resistivity, and longitudinal (maximal) wavefront voltage.

Results

Figure 1 shows a typical plot of time of activity for a beat initiated on the ventricular epicardium. Figure 2 plots conduction velocity vs. angle for the same electrode position. Theta (θ) is the angle between the line connecting stimulation and recording points and the fiber direction. Conduction velocities from the map in Figure 1 ranged from 21 cm/sec across fibers to 53 cm/sec along fibers, and are well correlated with angle. The solid curves in Figure 2 are (1) the velocity for an elliptical wave with a semimajor axis of v_l = 53 cm/sec (the mean of the observed velocities shown for $\theta < 5°$) and a semiminor axis of v_t = 22 cm/sec, calculated from the observed value of v_l and from the mean value of v_t/v_l reported below; and (2) the shape expected on the basis of the theory developed in the Appendix, again taken from the observed v_l = 53 cm/sec and the mean values of v_t/v_l, r_t/r_l, and wavefront voltage reported below. Clearly, our data are not sufficient to show which curve gives the better prediction.

Velocity of conduction for the seven dogs studied in which the stimulus length was less than 1 msec was: v_l = 58 ± 8 cm/sec; v_t = 25 ± 3 cm/sec; v_t/v_l = 0.42 ± 0.04. For the other two dogs, we used a longer stimulus duration, which made velocity calculations hazardous.

Figure 3 shows a potential map for the same electrode position as in Figure 1 at 10 msec after stimulation. Note the positive potentials before local depolarization along the fibers and the negative potentials laterally. Baruffi et al. (1978) have obtained epicardial potential maps similar to that in Figure 3. The uniform double-layer theory predicts zero potential outside a closed wavefront (Corbin and Scher, 1977). The wavefront under discussion

Downloaded from http://ahajournals.org by on March 12, 2022

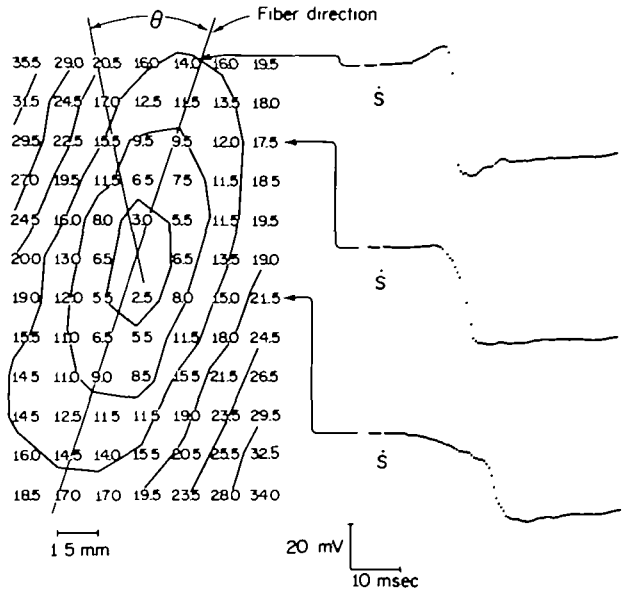

FIGURE 1 *Times of activity (msec) on the ventricular epicardium for the spread of the depolarization wave away from a central stimulation point. Theta (θ) is the angle between the fiber direction and the line connecting stimulating and recording points. The arrows indicate the position where each of the three waveforms on the right was recorded. Stimulus artifact is above the letter "S." Note that the shape of the waveforms depends on the angle θ. Longitudinal waves show positive potentials before local depolarization and rapid intrinsic deflections (upper waveform). Transverse waveforms (lower) show negative potentials before local depolarization and less rapid intrinsic deflections. Discussion in text.*

here is effectively closed, since the edges of the wavefront are in contact with an insulator. This is discussed below.

Figure 4A illustrates our definition of "wavefront voltage." This voltage was chosen to be the maximal voltage difference between points recorded an interval T apart, where T = 2 msec. Other choices for the time interval T result in other values of wavefront voltage, as illustrated in Figure 4B. We defer consideration of wavefront voltage measurement to the Discussion. For T = 2 msec, the data points illustrated in Figure 4C result for the same electrode position used in Figures 1 through 3.

The prediction labeled "Equation 1" in Figure 4C was fit to the experimentally determined longitudinal wavefront voltage V_{ol}. The variable V_{ot} in Equation 1, however, depends on no other voltage measurement, but was calculated from Equation 2 and the mean values of conduction velocity and tissue resistivity reported in this section. The agreement between the curve labeled "Equation 1" and the measured wavefront voltages over the entire range of the angle θ tends to confirm the prediction given by Equations 1 and 2.

In most cases, plots of wavefront voltage vs. θ showed more scatter and a smaller ratio of transverse-to-longitudinal wavefront voltage than was the case for the electrode position used for Figures 1 through 5. Let V_{ol} be the mean of the wavefront voltages (as defined above and in the legend to Figure 4) for $\theta < 10°$, and V_{ot} be the mean for $\theta > 80°$. Then, for the wavefront voltages graphed in Figure 4C we have $V_{ol} = 54$ mV, $V_{ot} = 15$ mV, and $V_{ol}/V_{ot} = 3.6$. For 24 electrode positions on nine dogs, we found $V_{ol} = 46 \pm 18$ mV (248 waveforms), $V_{ot} = 22 \pm 11$ mV (152 waveforms), and $V_{ol}/V_{ot} = 2.1$. We believe that the scatter in wavefront voltage measurements for many electrode positions may have been due to the presence of superficial blood vessels or to small amounts of fluid under the electrode.

The predicted curves in Figure 4 are given in terms of the angle θ, whereas the prediction of Equation 1 is in terms of the angle γ. The two angles have been defined above, and the relationship between them is explained in Appendix E.

Figure 5 is a map of the potentials induced by a 3-msec rectangular current pulse injected at the epicardial surface. The method used to determine the resistivities r_l and r_t was to choose a convenient isopotential on a plot such as Figure 5 and to measure with a ruler the longitudinal and transverse distances between the stimulation point and the isopotential line. Using Equation 21 (Appendix F), we could calculate the following resistivities.

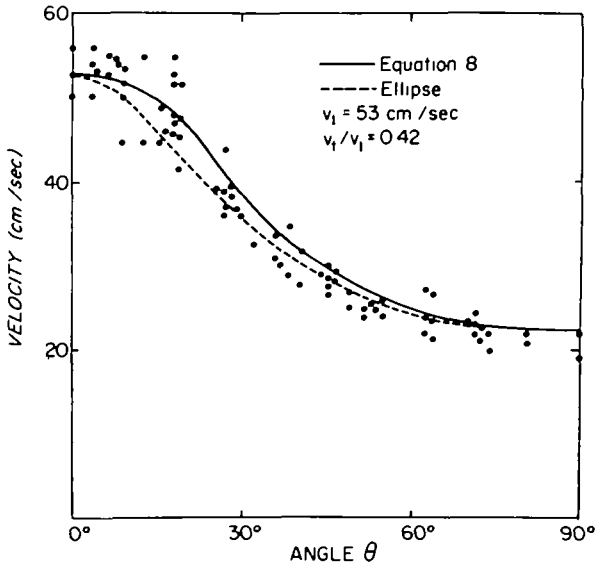

FIGURE 2 *Velocities as a function of θ, calculated from the times of activity given in Figure 1 by dividing the distance between recording and stimulating terminals by the time. The two calculated curves were fit to the observed velocities for this electrode position near θ = 0°; v_l is the longitudinal (γ = 0°) velocity and was determined by taking the mean of the illustrated points for θ < 5°; v_t/v_l is the ratio of transverse-to-longitudinal velocity. The mean value (0.42) of v_t/v_l for all nine dogs studied was used to calculate the two curves. Discussion in text.*

Downloaded from http://ahajournals.org by on March 12, 2022

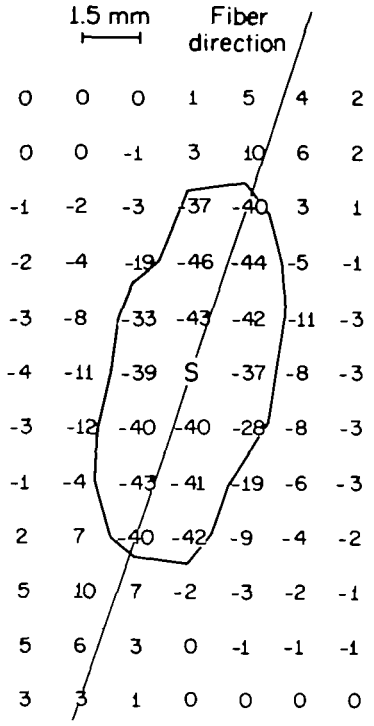

FIGURE 3 *Potential field (mV) 10 msec after stimulation. The depolarization wave has moved to the position shown by the heavy curve, which is the 10-msec isochrone in Figure 1. Note the asymmetry of the potentials outside the wavefront, the positive potentials ahead of the wave along the fiber direction, and the negative potentials in the transverse direction.*

There was no significant difference for resistivity to superthreshold vs. subthreshold current pulses. For the five dogs on which resistivity measurements were made, we found the values $r_l = 199 \pm 21$ Ω-cm, $r_t = 625 \pm 76$ Ω-cm, and $r_t/r_l = 3.16$ for the longitudinal and transverse resistivities. Using these resistivity values and the values of wavefront voltage from Figure 4, we can calculate the following values of intracellular (i), extracellular (o), longitudinal (l), and transverse (t) resistivity (in Ω-cm): $r_{ol} = 450$, $r_{ot} = 750$, $r_{il} = 360$, and $r_{it} = 3800$. The calculation is presented in Appendix D.

Discussion

These data indicate that there is a strong interdependence between epicardial fiber direction, conduction velocity, resistivity of the myocardium, and the potential field surrounding and generated by a wave of depolarization. Fiber direction has major effects on all of these variables. We consider these factors separately below.

Conduction Velocity

Our measurements of conduction velocity are in agreement with some measurements in the literature, but our results appear to be more reproducible than those in some previous studies. Our values for

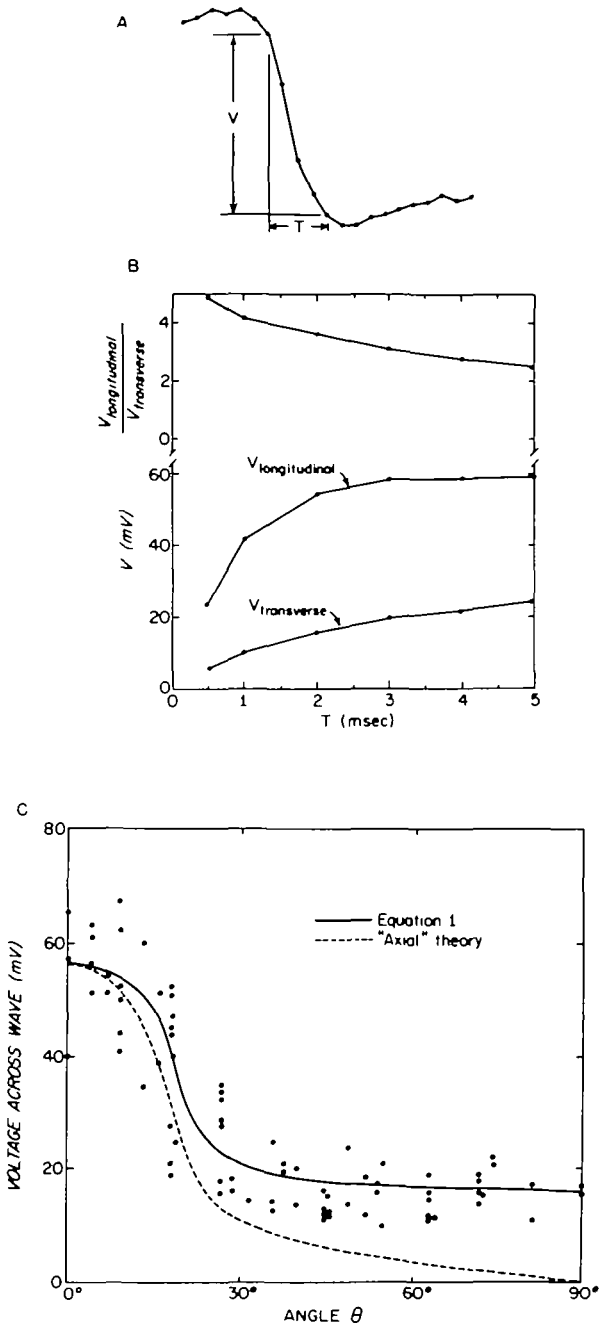

FIGURE 4 *A: Illustration of the method used for determining wavefront voltage. For each waveform, V is the maximal difference between potentials recorded an interval T apart. $V_{longitudinal}$ is the mean of the voltages V for angles θ < 10° (15 waveforms), and $V_{transverse}$ is the mean for θ > 80° (four waveforms) for the electrode position illustrated in Figures 1 through 3. B: $V_{longitudinal}$ is approximately the same for 2 < T < 5 msec, whereas $V_{transverse}$ continues to increase as T increases. C: The wavefront voltages V at each recording point, with T = 2 msec. The predictions of Equation 1 and of the "axial theory" are also shown. These curves were fit to the experimental data near θ = 0°, but the remaining experimental wavefront voltages were not used in calculating the curves (see text).*

Downloaded from http://ahajournals.org by on March 12, 2022

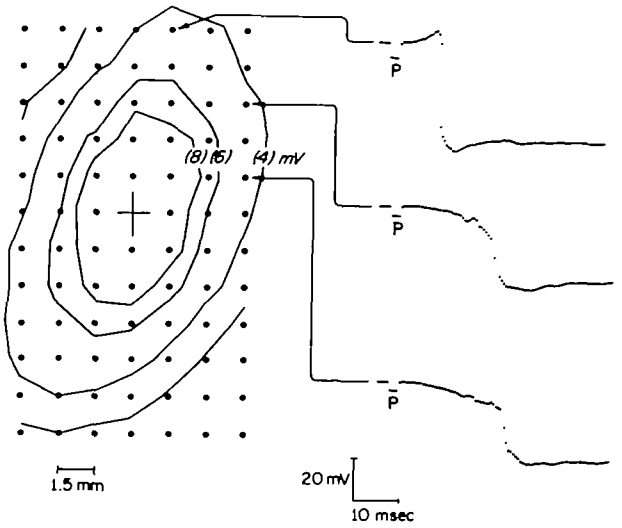

FIGURE 5 *Potentials (P) induced by a rectangular pulse of current injected at the central terminal. Lines join points of equal induced potential. The magnitude of the current was −37.5 μ A. This current was superthreshold, as indicated by the recorded waveforms. The waveforms at right show that the depolarization potentials do not interfere with measurement of the voltage deflection P. The squareness of the induced voltage for subthreshold and superthreshold pulses indicates that the medium is resistive, and that the transient due to the charging of the membrane capacity near the central terminal has a negligible effect on the potentials P. Discussion in text.*

conduction velocity were (means ± SD) $v_l = 58 \pm 8$ cm/sec for longitudinal velocity, $v_t = 25 \pm 3$ cm/sec for transverse velocity, and $v_t/v_l = 0.42 \pm 0.04$. These results compare with $v_l = 75 \pm 9$ cm/sec in calf trabeculae at 37°C (Weidmann, 1970); $v_l = 48 \pm 12$ cm/sec, $v_t = 16 \pm 3$ cm/sec, and $v_t/v_l = 0.33$ in calf trabeculae at 25°C (Clerc, 1976); v_l = 7-71 cm/sec and v_t = 8-20 cm/sec in isolated strips of dog ventricle (Sano et al., 1959); $v_l = 63$ cm/sec in dog ventricular myocardium at 37°C (Draper and Mya-Tu, 1959); and $v_l = 60$ cm/sec and $v_t = 28$ cm/sec on the in situ canine epicardium (Baruffi et al., 1978). The values at 25°C are not directly comparable to velocities measured at 37°C (Sano et al., 1959; Curtis and Travis, 1951). Our longitudinal velocity values agree well with those of Weidmann and of Draper and Mya-Tu, who used endocardial tissue which may have contained Purkinje fibers. Our values agree very well with those of Baruffi et al., who used a preparation nearly identical with ours.

Myerburg et al. (1978) have recently measured velocity on superfused canine endocardium. They report velocities $v_l = 98 \pm 25$ cm/sec, and $v_t = 25 \pm 13$ cm/sec for superficial endocardial ventricular muscle, and average conduction velocities in deep ventricular muscle of 26 ± 6 cm/sec. Their work suggests that there are differences in conduction velocity among different regions of the ventricular myocardium. Unfortunately, it appears to be difficult, with their superfused endocardial preparation, to strip away superficial muscle so as to expose deep ventricular muscle with a clearly defined fiber orientation. Other work (Selvester et al., 1970) has shown transmural variations in myocardial conduction velocity.

Gross Tissue Resistivity

Our method of resistivity measurement (Appendix F) is similar to the four-electrode technique of Rush et al. (1963). In both cases, the potential induced by a known current is measured. The technique used by Rush et al. (1963) may be less sensitive to boundary effects and to indifferent electrode placement. However, our potential-mapping method gives potentials at many distances from the current injection electrode, whereas the method of Rush et al. (1963) gave measurements of the potentials at fixed distances from the points at which current was injected and collected. In their study, current was injected and collected between two current electrodes 1.5 cm apart, and voltage was recorded from two electrodes each 0.5 cm from a current electrode and from each other (S. Rush, personal communication). This arrangement may lead to penetration of current deep into the myocardium, where fiber orientation is substantially different from that on the epicardium (Streeter et al., 1969; Armour and Randall, 1970). The distance between recording electrodes was greater than in our study. This may account for the somewhat higher anisotropy of resistivity found in the present work. Our values (in Ω-cm; means ± SD) of $r_l = 199 \pm 21$, $r_t = 625 \pm 76$, and $r_t/r_l = 3.16 \pm 0.16$ compare with the values given by Rush et al. (1963) of $r_l = 252 \pm 76$, $r_t = 563 \pm 84$, and $r_t/r_l = 2.2$. For in vitro preparations of mammalian trabeculae, these values have been reported: $r_l = 152 \pm 39$ (Weidmann, 1970); and $r_l = 125$, $r_t = 391$, $r_t/r_l = 3.1$, which can be calculated from the results of Clerc (1976).

Potentials around the Wavefront; Wavefront Voltage

The uniform double-layer theory predicts that there would be zero potential outside the three-dimensional wave whose intersection with the epicardium is shown in Figure 3, since the epicardium was bounded by air, which is an insulator, and thus there is no return current path around the wave. The potentials outside the wave are nonzero, indicating that the uniform double-layer theory is inadequate for prediction of these potentials.*

One difficulty in the interpretation of maps such

* We assume that there is no extracardiac return current path. Even if the layer (100 μm thick, determined from histological sections) of superficial epicardial connective tissue and any epicardial fluid provide a return path, the asymmetry of the potential field outside the boundary between resting and depolarized tissue shows that the uniform double-layer theory is inadequate.

Downloaded from http://ahajournals.org by on March 12, 2022

as that in Figure 3 is that the wavefront thickness is unknown. For example, negative potentials outside the isochrone in the transverse direction might be found if the recording point were partly "inside" the depolarization wavefront.

However, the positive potentials preceding local depolarization ("approaching positivity") in recordings from fibers excited longitudinally are not difficult to interpret. A series of potential maps such as that in Figure 3 shows that the magnitude of the peak approaching positivity is not systematically related to the distance from the stimulating terminal over the 9 × 16.5-mm area of the epicardial electrode. This indicates that the wavefront thickness did not seriously affect the observed approaching positivity. If measurements were made later than 35 or 40 msec after stimulation, the epicardial potentials would be drastically different, since the wave would break through on the endocardium and the wavefront would no longer be closed. We did not study potential maps later than 20 msec after stimulation.

Our results confirm the inequality of wavefront voltage (Clerc, 1976; Corbin and Scher, 1977) for transverse vs. longitudinal wave propagation. There is, however, some difference between the extracellular potential drop we found across the wave and the results of Weidmann (1970) and Clerc (1976). Weidmann found a mean extracellular value of 21 mV across waves moving longitudinally in sheep and calf trabeculae. In the same preparation, Clerc found values of 20 mV for longitudinal propagation and 7 mV for transverse propagation. (These values measured by Weidmann and Clerc are calculated from the resistivity values reported by these authors and an assumed action potential magnitude of 100 mV.) The longitudinal wavefront voltage reported in the Results was 46 mV, and Vander Ark and Reynolds (1970) found a mean peak-to-peak voltage for longitudinal waves of 74 mV. These measurements were on the canine epicardium. We do not understand why wavefront voltage in the studies of Weidmann and of Clerc is lower than that measured on the canine epicardium.

We shall outline here some of the difficulties in measurements of the wavefront voltages V_{ol}, V_{ot}, and $V_o(\gamma)$, and will attempt to justify the technique we have chosen for these measurements. That technique (see Methods) was to take for each recorded waveform the maximal potential difference between points recorded 2 msec apart.

Examination of the waveforms in Figure 1 reveals the difficulty in identifying the "wavefront voltage." The potential change during local depolarization (intrinsic deflection) is not sufficiently rapid to be clearly distinguishable from slower potential changes due to the motion of distant parts of the wave. The justification for identifying wavefront voltage with unipolar potential change over a fixed time interval is as follows. As predicted by Clerc (1976), the time course of the propagated action potential should be the same regardless of the angle of propagation. [In support of this prediction, the maximal rate of change of the action potential is the same for different angles of propagation (Myerburg et al., 1978).] Hence, the depolarization wave should take the same time to pass a recording point, whatever the angle of propagation. The choice of 2 msec as the time interval for determining wavefront voltage is consistent with estimates of the thickness of the wavefront (Vander Ark and Reynolds, 1970), with estimates of the duration of the rising phase of the action potential in ventricle (Weidmann, 1956), with the detailed shape of the rising phase of the action potential (Chen et al., 1975), and with our observations of the duration of the intrinsic deflection (see, for example, the upper waveform in Figure 1). In addition, this measurement correlates well with maximal potential differences over 0.5 (r = 0.975), 1.0 (r = 0.990), and 3.0 msec (r = 0.995) for the case illustrated in Figure 4.

It might be argued that a less arbitrary method of wavefront voltage measurement would be preferable to the one used in this study. For example, the peak-to-peak amplitude of the unipolar waveform could be used. We believe, however, that unipolar peak-to-peak voltage magnitude is an inappropriate index of wavefront voltage in myocardium and tends to obscure rather than reveal variations of this voltage due to fiber orientation. Our basis for this belief is that, whereas the peak-to-peak magnitude is equal to the wavefront voltage for a wave propagating longitudinally from a point of stimulation, the peak-to-peak voltage is much larger than the wavefront voltage for a wave propagating transversely. The reason for this difference can be seen in the waveforms in Figure 1. For the upper waveform (longitudinal wave), the peak-to-peak voltage is approximately equal to the maximal potential change over 2 msec, so that these two measures of wavefront voltage agree. The peaks occur 5 msec apart. For the lower waveform (transverse wave) the peak-to-peak voltage is much greater than the maximal change over 2 msec, and the peaks occur at least 30 msec apart. The difference between potentials recorded 30 msec apart reflects the wavefront voltages over a large area of the wave, not local wavefront voltage. The inadequacy of peak-to-peak voltage as a measure of wavefront voltage also can be seen from theoretical simulations of potential fields in heart: a simulation of the extracellular wave forms recorded near a spherical wave with an assumed anisotropic wavefront strength shows that the peak-to-peak voltage at a given recording point may be unrelated to the voltage of the wave that passes that recording point (Corbin and Scher, 1977). Thus, peak-to-peak voltage is not in general equal or proportional to the wavefront voltage.

Another potential problem in resolving details of

Downloaded from http://ahajournals.org by on March 12, 2022

the extracellular waveform during depolarization is the finite size of the recording terminal. The terminals on the epicardial array electrode (see Methods) were 250 μm in diameter. The time required for the wave to travel 250 μm is approximately 0.4 msec for a longitudinal wave and 1.0 msec for a transverse wave (distance/velocity), so the maximal potential change over 2.0 msec (used in this study for wavefront voltage measurement) should be only slightly affected by the size of the recording terminals. Records made with a smaller terminal (diameter 75 μm) did not differ appreciably from those made with the 250-μm terminals, and thus indicated that the latter were sufficiently small for this study.

The experimental studies reported here do not provide a basis for asserting the quantitative accuracy of Equations 1 and 2. The strongest evidence against the validity of the uniform double-layer model is still direct experimental measurements, such as are given in Figures 3 and 4. However, in view of the model proposed by Weidmann (1970) for the magnitude of the wavefront voltage, of the changes in resistivity with fiber direction (Rush et al., 1963), and of the great anatomical anisotropy at the cellular level, it would be an unlikely coincidence if the wavefront voltage did not vary greatly for different directions of propagation.

Frank (1953) pointed out that it should be possible to represent the depolarization wave in the myocardium with a distributed current-dipole layer. This possibility is not challenged by our experimental results, but the hypothesis that the double-layer is uniform is challenged. Our results show that the voltage across a wave moving longitudinally is roughly three times as great as the voltage across a wave moving transversely. Since the gross tissue conductivity is three times as great in the longitudinal direction, the equivalent double-layer strength (dipole moment per unit area of the wave) producing the extracellular voltage drop across the wave is about $3 \times 3 = 9$ times as great for a wave moving longitudinally as for a wave moving transversely. That is, the membrane currents generating the extracellular voltage drop across the wave must maintain a voltage three times higher against a resistance three times lower for a longitudinal wave, which requires nine times the equivalent dipole moment per unit area.

We have not calculated here the equivalent dipole moment of a depolarization wave as a function of angle between the wave and local fiber direction, nor have we calculated the potential field that would be produced by a dipole in an anisotropic medium such as myocardium. Such calculations would be needed for a prediction of extracellular potentials at a distance from a depolarization wave. We believe that the tissue model presented in the Appendix provides a basis for calculation of these equivalent sources. We have shown that in certain cases the uniform double-layer model for the electrical sources in myocardium is insufficient for prediction of extracellular potentials. It appears certain that the effects of anisotropic conductivity and wavefront voltage will have to be considered if the potentials around local segments of depolarizing myocardium are to be understood. It remains to be seen how important these effects will be in understanding the body surface electrocardiogram.

Appendix

The following notation will be used in the Appendix:

- V = potential (V)
- Δ = membrane action potential (V)
- $\vec{J}$, J = current density, vector or scalar (A/cm^2)
- I = current (A)
- v, u = velocity (cm/sec)
- r = resistivity (Ω-cm)
- σ = conductivity (mho/cm)
- x, y, z = distance (cm)
- γ = angle between a line drawn perpendicular to a wavefront and the long axis of local muscle fibers
- θ = angle between a line drawn from stimulation point to recording point, and the long axis of local muscle fibers
- λ = tissue space constant (cm)

Subscripts:

- l = longitudinal
- t = transverse
- i = intracellular
- o = extracellular

The definitions of the angles θ and γ are illustrated in Figure 6.

A. Model of Tissue Electrical Properties; Resistivities

Our tissue model represents myocardium by two parallel, continuous, three-dimensional, anisotropic conducting media, the extracellular and intracellular media. Current flow in the two media follows Ohm's law: $\vec{J}_i = -\sigma_i \nabla V_i$ for the intracellular medium, and $\vec{J}_o = -\sigma_o \nabla V_o$ for the extracellular medium; σ_i and σ_o are second-rank tensors (Landau and Lifshitz, 1960), each with one principal axis along the local fiber direction. The conductivity is assumed to be the same in the two transverse directions, so the tensors σ_i and σ_o are diagonal when any coordinate axis is aligned with the fiber direction.

For calculations concerning wavefront voltage (Appendix C) and potential induced by an injected current pulse (Appendix F), some additional assumptions will be made. For wavefront voltage calculations, we will not be concerned with details of the time dependence of the voltage very close to the time of local depolarization, so we will idealize these potentials as changing instantaneously as the wavefront passes a given point. That is, we treat

Downloaded from http://ahajournals.org by on March 12, 2022

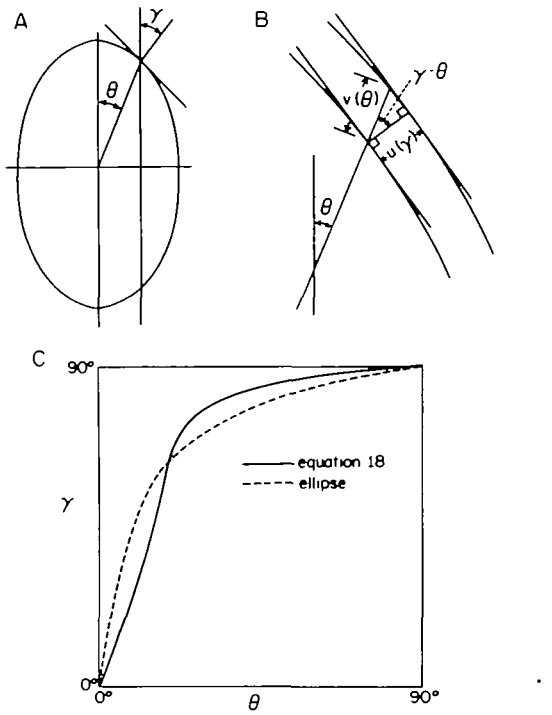

FIGURE 6 *The relationship between the ray velocity u(θ) and the wavefront velocity v(γ) for a wave with anisotropic conduction velocity. A: The definition of the angles θ and γ. B: An expanded view of the wave at two times separated by a very small time interval, showing the relationship between u(θ) and v(γ). C: The correspondence between the angles θ and γ for an ellipse with a short axis 0.42 times as long as its long axis, and for the velocity function v(γ) predicted by Equation 8 for the same ratio of axis lengths, and for the other parameters given in the text (see Appendix C).*

the wave as being perfectly smooth, and the cell membrane as being a voltage source generating the resting potential "ahead" of the wave (i.e., in tissue not yet depolarized) and generating the plateau potential for membrane "behind" the wave (i.e., in tissue already depolarized). The assumption that the membrane is a voltage source is equivalent to the assumption that the space constant λ is zero. Since λ is less than 1 mm for resting tissue (Weidmann, 1970), the assumption that $\lambda = 0$ is adequate, provided measurements are made more than a few millimeters from any current source. For example, the method of resistivity measurement described in Appendix F requires that the recording points be far enough from the current source terminal that the space constant can be taken to be zero with negligible error. Properties of the tissue beyond those included in this simple model are implicit in Equation 7 below, which we have taken from the literature.

We shall work below with reciprocals of elements of the tensors σ_i and σ_o. The four resistivities r_{il}, r_{ol}, r_{it}, and r_{ot} are the intracellular and extracellular, longitudinal and transverse resistivities. For example, r_{il} is defined to be $r_{il} = (dV_i/dx)/J_i$, where x is distance in the longitudinal direction. That is, r_{il} is the potential gradient divided by the resultant current density. Here J_i is the current density per area of tissue, not per area of intracellular space. Defined in this way, the resistivities are independent of any assumption about the fraction of the tissue that is intracellular and the fraction that is extracellular. [We emphasize this point because some resistivity values have been reported in terms of the specific resistivity of intracellular and extracellular fluid (Weidmann, 1970; Clerc, 1976). These depend on determination of relative volumes of intra- and extracellular space.]

We shall use the notation r_l and r_t for the longitudinal and transverse resistivities of the tissue, respectively, and we will call these "gross tissue resistivity." These are the parallel combination of intracellular and extracellular resistivities:

$$r_l = r_{ol}r_{il}/(r_{ol} + r_{il}), \quad (3)$$

$$r_t = r_{ot}r_{it}/(r_{ot} + r_{it}). \quad (4)$$

The longitudinal and transverse resistivities influence the propagation of waves moving longitudinally or transversely. For a plane wave moving at an angle γ intermediate between 0° and 90°, the component of resistivity perpendicular to the wavefront must be known:

$$r_o(\gamma) = r_{ol}/[\cos^2\gamma + (r_{ol}/r_{ot})\sin^2\gamma], \quad (5)$$

$$r_i(\gamma) = r_{il}/[\cos^2\gamma + (r_{il}/r_{it})\sin^2\gamma]. \quad (6)$$

The resistivities $r_o(\gamma)$ and $r_i(\gamma)$ are the reciprocals of diagonal elements of the conductivity tensors σ_i and σ_o, and are obtained by applying a rotation operator (Morse and Feshbach, 1953) to the diagonal form of σ_i and σ_o. For $\gamma = 0°$ (longitudinal), Equations 5 and 6 reduce to $r_o(0°) = r_{ol}$ and $r_i(0°) = r_{il}$. For $\gamma = 90°$ (transverse), Equations 5 and 6 reduce to $r_o(90°) = r_{ot}$ and $r_i(90°) = r_{it}$.

Figure 7 is the model we will use for calculating wavefront voltage for a plane depolarization wave. For a longitudinal wave, we substitute in Figure 7 r_{ol} and r_{il} for r_o and r_i, respectively. Similarly, for a transverse wave, we substitute r_{ot} and r_{it}. For a plane wave whose perpendicular makes an angle γ with fiber direction, we can insert $r_o(\gamma)$ and $r_i(\gamma)$ from Equations 5 and 6.

B. Conduction Velocity

Transverse and longitudinal conduction velocities are related to the resistivities as follows:

$$\frac{v_t}{v_l} = \left(\frac{r_{il} + r_{ol}}{r_{it} + r_{ot}}\right)^{1/2}. \quad (7)$$

Clerc (1976) derives this formula by assuming equality of the time constant τ_{foot}, characterizing the foot of the action potential for longitudinal and transverse conduction. This conclusion is analogous

Downloaded from http://ahajournals.org by on March 12, 2022

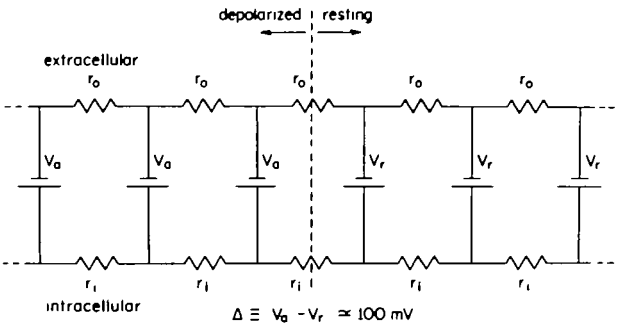

FIGURE 7 *Model used for calculating extracellular voltage drop across a plane depolarization wave. The batteries represent the membrane potential. The values of r_i and r_o depend on the angle between the propagation direction and the fiber direction (see Appendix C).*

to the conclusion that nerve conduction velocity should be proportional to the square root of the nerve radius (Hodgkin, 1954). Equation 7 for heart is perhaps more sound than that for nerve, since it depends on the assumption that the membrane properties remain the same. For heart, it is evident that the membrane properties remain the same as the direction of propagation is varied, since it is the same membrane. On the other hand, it appears unlikely that the nerve radius can vary without some change in the membrane properties.

Equation 7 can be extended to angles intermediate between longitudinal and transverse propagation by putting $r_o(\gamma)$ and $r_i(\gamma)$ from Equations 5 and 6 into Equation 7 in place of r_{ot} and r_{it}:

$$v(\gamma) = v_l\left(\frac{r_{il} + r_{ol}}{r_i(\gamma) + r_o(\gamma)}\right)^{1/2}. \quad (8)$$

The dependence on anisotropy of resistivity given in Equation 8 agrees with the prediction of a related model (Muler and Markin, 1977). According to Equation 8, the expected geometrical shape of a wave starting from a point of stimulation is nearly (but not exactly) an ellipsoid of revolution, so that the observed shape on the epicardium for epicardial stimulation is nearly an ellipse (if we neglect the rotation of fiber direction with depth into the myocardium). The accuracy of our velocity measurements is insufficient to distinguish the small difference between the predicted nonelliptical isochrone shape and a perfect ellipse (Fig. 2). Equation 8 predicts a spherical wave in the special case of isotropic tissue.

C. Wavefront Voltage

The extracellular potential drop during local depolarization depends on the size of the membrane action potential $\Delta = V_a - V_r \simeq 100$ mV, and on the resistivities r_o and r_i (see Fig. 7) (Weidmann, 1970; Clerc, 1976). We shall use the notation V_o for the extracellular potential drop across the wave of depolarization. From Figure 7,

$$V_o = \Delta[r_o/(r_i + r_o)]. \quad (9)$$

Writing in explicitly the dependence of r_o and r_i on the orientation angle γ, we obtain

$$V_o(\gamma) = \Delta\frac{r_o(\gamma)}{r_i(\gamma) + r_o(\gamma)}, \quad (10)$$

where $r_i(\gamma)$ and $r_o(\gamma)$ are given by Equations 5 and 6. This reduces to the formulas used by others (Weidmann, 1970; Clerc, 1976) for longitudinal and transverse propagation for the angles 0° and 90°, respectively:

$$V_{ol} = \Delta[r_{ol}/(r_{ol} + r_{il})], \quad (11)$$

$$V_{ot} = \Delta[r_{ot}/(r_{ot} + r_{it})]. \quad (12)$$

Equation 1 (see Methods) can be verified by inserting into it V_{ol} and V_{ot} from Equations 11 and 12, r_l and r_t from Equations 3 and 4, and $V_o(\gamma)$ from Equation 10, using in Equation 10 the expressions from Equations 5 and 6 for $r_o(\gamma)$ and $r_i(\gamma)$. With these substitutions, Equation 1 is shown to be an identity.

Equation 2 can be verified by substituting into it V_{ot} from Equation 12, V_{ol} from Equation 11, v_t/v_l from Equation 7, and r_l and r_t from Equations 3 and 4. With these substitutions, Equation 2 is an identity.

D. Calculation of r_{il}, r_{ol}, r_{it}, and r_{ot}

Equations 3, 4, 11, and 12 relate gross tissue resistivity and wavefront voltage to the resistivities r_{il}, r_{ol}, r_{it}, and r_{ot}. In this section, values of these resistivities will be calculated for use in calculations in Appendix E.

From Equations 3 and 11, we have

$$r_{il} = r_l\Delta/V_{ol}, \quad (13)$$

and from Equations 4 and 12, we have

$$r_{it} = r_t\Delta/V_{ot}. \quad (14)$$

From Equation 3,

$$r_{ol} = r_{il}r_l/(r_{il} - r_l), \quad (15)$$

and from Equation 4,

$$r_{ot} = r_{it}r_t/(r_{it} - r_t). \quad (16)$$

From the Results section, $r_l = 199$ and $r_t = 625$ ohm-cm. From Figure 4, taking the mean of the potential drops for angles less than 5°, we have $V_{ol} = 56$ mV. From the Results, $v_t/v_l = 0.42$. Equation 2 then gives $V_{ot} = 16$ mV, where $\Delta = 100$ mV. Equations 13 through 16 then give these resistivity values (ohm-cm): $r_{ol} = 450$, $r_{ot} = 750$, $r_{il} = 360$, and $r_{it} = 3800$.

As noted in Appendix A, some values of resistivity in the literature (Weidmann, 1970; Clerc, 1976) have been reported as specific resistivities, which are dependent on assumptions about relative volumes of intracellular and extracellular space. The

Downloaded from http://ahajournals.org by on March 12, 2022

resistivities above are expressed in the form explained in Appendix A.

E. Relation between Angles θ and γ

Waves with anisotropic conduction velocity may be characterized by ray velocity $u(\theta)$ or by wavefront velocity $v(\gamma)$ (Whitham, 1974). These velocities are illustrated in Figure 6. As can be seen from the figure,

$$v(\gamma) = u(\theta)\cos(\gamma - \theta). \quad (17)$$

The ray velocity $u(\theta)$ is the rate at which the wave moves along a line θ = constant from the point of origin of the wave. The wavefront velocity $v(\gamma)$ is the rate at which the wave moves along a line perpendicular to a plane tangent to the wavefront. A useful relationship between the angles θ and γ for any reasonable function $v(\gamma)$ is (Whitham, 1974)

$$\tan(\gamma - \theta) = -\frac{1}{v}\cdot\frac{dv}{d\gamma}. \quad (18)$$

It can be shown that the function $v(\gamma)$, which gives an elliptical geometrical shape for a wave starting from a point, is

$$v(\gamma) = v_l[\cos^2\gamma + (v_t/v_l)^2 \sin^2\gamma]^{1/2} \text{ (ellipse)}, \quad (19)$$

where v_l is the semimajor axis and v_t is the semiminor axis. Equation 18 can be solved analytically for this case. The result is

$$\theta = \arctan[(v_t/v_l)^2 \tan\gamma] \text{ (ellipse)}. \quad (20)$$

For the ratio $(v_t/v_l) = 0.42$ (see Results), Equation 20 gives the curve labeled "ellipse" in Figure 6C.

For the velocity function predicted for myocardium by Equation 8, Equation 18 gives the relationship between θ and γ labeled "Equation 18" in Figure 6C. In this calculation, $v(\gamma)$ from Equation 8 has been substituted into Equation 18 to give an implicit equation relating θ and γ, and the values of r_{ol}, etc., from Appendix D have been used.

The experimental results given in Figures 2 and 4 are presented in terms of the angle θ because this angle is experimentally easy to determine. It is simply the angle between the fiber direction and the line connecting the point of stimulation and the recording point.

F. Gross Tissue Resistivity

The potential V with respect to an indifferent electrode at infinity due to the injection of a current I at the coordinate origin into an infinite half-space $z > 0$ of an anisotropic medium in contact with a perfectly insulating half-space $z < 0$ is (Nicholson, 1973, Eq. 7)

$$V = \frac{r_t I}{2\pi R}, \quad (21)$$

where

$$R = [x^2 + (r_t/r_l)(y^2 + z^2)]^{1/2}. \quad (22)$$

Equation 21 is the appropriate form for the potential induced by a current injected at the epicardium ($z = 0$), since the fibers run parallel to the epicardial surface (Armour and Randall, 1970). It is assumed that the resistivity perpendicular to the epicardium is the same as the transverse resistivity parallel to the epicardium. The insulator over the heart is air or the plastic electrode body. The main practical difficulties in applying Equation 21 to the determination of tissue resistivities are: (1) the requirement that the indifferent electrodes for recording and current injection must be at great distance from the current injection point and from each other, and (2) the medium must be very large compared with the distance between the current injection point and the recording point. In our experiments, the current injection indifferent and recording indifferent electrodes were at remote sites on the dog's body.

Acknowledgments

We gratefully acknowledge the surgical and technical help of Roger Scott and the editorial assistance of Diane Clark.

References

Armour JA, Randall WC: Structural basis for cardiac function. Am J Physiol **218:** 1517–1523, 1970

Baruffi S, Spaggiari S, Stilli D, Musso E, Taccardi B: The importance of fiber orientation in determining the features of the cardiac electric field. *In* Modern Electrocardiology, edited by Z Antaloczy. Amsterdam, Excerpta Medica, 1978, pp 89–92

Chen CM, Gettes LS, Katzung BG: Effect of lidocaine and quinidine on steady-state characteristics and recovery kinetics of $(dV/dt)_{max}$ in guinea pig ventricular myocardium. Circ Res **37:** 20–29, 1975

Clerc L: Directional differences of impulse spread in trabecular muscle from mammalian heart. J Physiol (Lond) **255:** 335–346, 1976

Corbin LV II, Scher AM: The canine heart as an electrocardiographic generator: Dependence on cardiac cell orientation. Circ Res **41:** 58–67, 1977

Curtis HJ, Travis DM: Conduction in Purkinje tissue of the ox heart. Am J Physiol **165:** 173–178, 1951

Draper MH, Mya-Tu M: A comparison of the conduction velocity in cardiac tissues of various mammals. Q J Exp Physiol **44:** 91–109, 1959

Durrer D, van Dam RT, Freud GE, Janse MJ, Meijler FL, Arzbaecher RC: Total excitation of the isolated human heart. Circulation **41:** 899–912, 1970

Frank E: A comparative analysis of the eccentric double-layer representation of the human heart. Am Heart J **46:** 364–378, 1953

Hodgkin AL: A note on conduction velocity. J Physiol (Lond) **125:** 221–224, 1954

Kehl TH, Moss CM, Dunkel L: LM²—a logic machine minicomputer. Computer **8:** 12–22, 1975

Landau LD, Lifshitz EM: Electrodynamics of Continuous Media. Reading, Mass., Addison-Wesley, 1960

MacInnes DA: The Principles of Electrochemistry. New York, Dover, 1961

Morse PM, Feshbach H: Methods of Theoretical Physics. New York, McGraw-Hill, 1953, p 63

Muler AL, Markin VS: Electrical properties of anisotropic nerve-muscle syncytia: II. Spread of flat front of excitation. Biofizika **22:** 518–522, 1977 (English translation: Biophysics **22:** 536–541, 1977)

Myerburg RJ, Gelband H, Nilsson K, Castellanos A, Morales AR, Bassett AL: The role of canine superficial ventricular muscle fibers in endocardial impulse distribution. Circ Res **42:**

Downloaded from http://ahajournals.org by on March 12, 2022

27-35, 1978
Nicholson C: Theoretical analysis of field potentials in anisotropic ensembles of neuronal elements. IEEE Trans Biomed Eng **20:** 278-288, 1973
Plonsey R: An evaluation of several cardiac activation models. J Electrocardiol **7:** 237-244, 1974
Rush S, Abildskov JA, McFee R: Resistivity of body tissues at low frequencies. Circ Res **12:** 40-50, 1963
Sano T, Takayama N, Simamoto T: Directional difference of conduction velocity ion the cardiac ventricular syncytium studied by microelectrodes. Circ Res **7:** 262-267, 1959
Scher AM, Young AC: Ventricular depolarization and the genesis of QRS. Ann NY Acad Sci **65:** 768-778, 1957
Selvester RH, Kirk WL Jr, Pearson RB: Propagation velocities and voltage magnitudes in local segments of dog myocardium. Circ Res **27:** 619-629, 1970
Sodi-Pallares D: New Bases of Electrocardiography. St. Louis, CV Mosby, 1956
Spach MS, Barr RC: Cardiac anatomy from an electrophysiological viewpoint. *In* The Theoretical Basis of Electrocardiology, edited by CV Nelson, DB Geselowitz. Oxford, Clarendon Press, 1976, pp 3-20
Streeter DD Jr, Spotnitz HM, Patel DP, Ross J Jr, Sonnenblick EH: Fiber orientation in the canine left ventricle during diastole and systole. Circ Res **24:** 339-347, 1969
Vander Ark CR, Reynolds EW: An experimental study of propagated electrical activity in the canine heart. Circ Res **26:** 451-460, 1970
Weidmann S: Elektrophysiologie der Herzmuskelfaser. Bern, Huber, 1956, p 25
Weidmann S: Electrical constants of trabecular muscle from mammalian heart. J Physiol (Lond) **210:** 1041-1054, 1970
Whitham GB: Linear and Nonlinear Waves. New York, Wiley, 1974, pp 257-259

The Influence of Left Ventricular Filling on Postextrasystolic Potentiation in the Dog Heart

EDWARD L. YELLIN, ARTHUR KENNISH, CHAIM YORAN, SHLOMO LANIADO, NANCY M. BUCKLEY, AND ROBERT W.M. FRATER

SUMMARY **We studied the role of left ventricular filling on postextrasystolic potentiation (PESP) in the intact dog heart by calculating changes in end-systolic and end-diastolic volumes on a beat-to-beat basis from electromagnetic measurements of phasic mitral inflow and aortic outflow. In all, 161 extrasystolic sequences with compensatory pauses in 13 dogs were analyzed. The first postextrasystolic cycle showed an increased end-diastolic volume (EDV) in 94%, a decreased end-systolic volume (ESV) in 50%, and an estimated increased ejection fraction in 85% of the sequences. In the 91 sequences with a coupling index ≤0.7, despite a 76% increase in filling time, there was during the compensatory pause only a 6% increase in filling volume when compared to control. The net filling volume, stroke volume, and diastolic filling period for the sum of the extra- and postextrasystolic cycles were, respectively, 78%, 80%, and 116% of the sum of two control cycles. This retarded filling rate is attributed to a lower left atrial pressure, a reduced left ventricular relaxation rate, and a relaxation to a higher pressure minimum, all of which decrease the amplitude of the atrioventricular pressure gradient. Nevertheless, in 98% of the postextrasystolic cycles, stroke volume was augmented when compared to control (ratio, 1.49 ± 0.26; mean ± SD), due in part to intrinsic mechanisms, to increased preload (EDV), and to decreased afterload. As a first approximation, the effects of increases in preload were separated from intrinsic increases in contractility following an extrasystole by defining potentiation in terms of decreased ESV and/or increased ejection fraction. With the former criterion, 50% of the sequences showed PESP; with the latter, PESP occurred in 85% of the sequences.** ***Circ Res 44: 712-722, 1979***

Downloaded from http://ahajournals.org by on March 12, 2022

STUDIES IN isolated muscle preparations (Cranefield, 1965) and isovolumic ventricles (Cranefield, 1965; Hoffman et al., 1965) with controlled preload have shown that extrasystoles give rise to increases in the magnitude of developed tension and in the rate of development of tension in subsequent contractions. Postextrasystolic potentiation (PESP) is clearly an intrinsic property of cardiac muscle and is independent of afterload and preload.

In the intact, ejecting heart, postextrasystolic increases in peak left ventricular pressure (PLVP), maximum dp/dt, and stroke volume (SV) also have been demonstrated clearly. (Cranefield, 1965; Hoffman, et al., 1965; Takada et al., 1970; Anderson et al., 1976). However, the influence of ventricular filling on PESP in the intact heart has never been

From the Departments of Surgery and Physiology, Cardiovascular Research Laboratory, Albert Einstein College of Medicine, Bronx, New York.

Supported in part by National Heart, Blood, and Lung Institute Grant HL 19391.

Address for reprints: Edward L. Yellin, Ph.D., Department of Surgery, Albert Einstein College of Medicine, 1300 Morris Park Avenue, Bronx, New York, 10461.

Received May 23, 1978; accepted for publication December 6, 1978.